Applications of Computational Mechanics in Geotechnical Engineering – Sousa, Fernandes, Vargas Jr & Azevedo (eds)
© 2007 Taylor & Francis Group, London, ISBN 978-0-415-43789-9

Numerical simulations of materials with micro-structure: limit analysis and homogenization techniques

P.B. Lourenço
University of Minho, Department of Civil Engineering, Guimarães, Portugal

ABSTRACT: Continuum-based numerical methods have played a leading role in the numerical solution of problems in soil and rock mechanics. However, for stratified soils and fractured rocks, a continuum assumption often leads to difficult parameters to define and over-simplified geometry to be realistic. In such cases, approaches that consider the micro-structure of the material can be adopted. In this paper, two of such approaches are detailed, namely limit analysis incorporating fractures and individual blocks, and elastoplastic homogenization of layered soils.

1 INTRODUCTION

The present paper addresses the inelastic behavior of heterogeneous media, such as soils and rocks. This problem can be, basically, approached from two directions. A possible direction is to gather, collate and interpret extensive experimental data and, ultimately, manipulate it in the form of master curves in terms of non-dimension variables. One step further can be to seek empirical analytical expressions that fit the experimental data. However, this approach will not be followed here. Even tough such an approach can be useful, the results are limited to the conditions under which the data were obtained. New materials and/or application of a well known material in different loading conditions lead to a new set of costly experimental programs. Here, a more fundamental approach, with a predictive nature, is sought using two different tools, namely limit analysis and homogenization techniques.

2 LIMIT ANALYSIS

A continuum assumption can lead to difficult parameters to define and over-simplified geometry to be realistic, particularly in the case of fractured rocks. At least in such case, discrete representations of fractures and individual blocks must be adopted. Different approaches are possible to represent these heterogeneous media, namely, the discrete element method (DEM), the discontinuous finite element method (FEM) and limit analysis (LAn).

The explicit formulation of a discrete (or distinct) element method is detailed in the introductory paper by Cundall and Strack (1985). The discontinuous deformation analysis (DDA), an implicit DEM formulation, was originated from a back-analysis algorithm to determine a best fit to a deformed configuration of a block system from measured displacements and deformations, Shi and Goodman (1985). The relative advantages and shortcomings of DDA are compared with the explicit discrete element method and the finite element method (Hart, 1991), even if significant developments occurred in the last decade, particularly with respect to three-dimensional extension, solution techniques, contact representation and detection algorithms. The typical characteristics of discrete element methods are: (a) the consideration of rigid or deformable blocks (in combination with FEM); (b) connection between vertices and sides/faces; (c) interpenetration is usually possible; (d) integration of the equations of motion for the blocks (explicit solution) using the real damping

coefficient (dynamic solution) or artificially large (static solution). The main advantages are an adequate formulation for large displacements, including contact update, and an independent mesh for each block, in case of deformable blocks. The main disadvantages are the need of a large number of contact points required for accurate representation of interface stresses and a rather time consuming analysis, especially for 3D problems.

The finite element method remains the most used tool for numerical analysis in solid mechanics and an extension from standard continuum finite elements to represent jointed rock was developed in the early days of non-linear mechanics, Goodman *et al.* (1967). On the contrary, limit analysis received far less attention from the technical and scientific community for jointed rock, while being very popular for soil problems, Fredlund and Krahn (1977). Still, limit analysis (kinematic approach) has the advantage of being a simple tool, while having the disadvantages that only collapse load and collapse mechanism can be obtained and loading history can hardly be included. Here, a novel implementation of limit analysis is detailed and applied to an illustrative example.

2.1 *General formulation*

The limit analysis formulation for a rigid block assemblage detailed next adopts the following basic hypotheses: the joint between two blocks can withstand limited compressive stresses and the Coulomb's law controls shear failure, which features non-associated flow given by a zero dilatancy angle.

The static variables, or generalized stresses, at a joint k are selected to be the shear force, V_k, the normal force, N_k, and the moment, M_k, all at the center of the joint. Correspondingly, the kinematic variables, or generalized strains, are the relative tangential, normal and angular displacement rates, δn_k, δs_k and $\delta\theta_k$ at the joint center, respectively. The degrees of freedom are the displacement rates in the x and y directions, and the angular change rate of the centroid of each block: δu_i, δv_i and $\delta\omega_i$ for the block i. In the same way, the external loads are described by the forces in x and y directions, as well as the moment at the centroid of the block. The loads are split in a constant part (with a subscript c) and a variable part (with a subscript v): f_{cxi}, f_{vxi}, for the forces in the x direction, f_{cyi}, f_{vyi}, for the forces in the y direction, and m_{ci}, m_{vi}, for the moments. These variables are collected in the vectors of generalized stresses $\mathbf{Q}$, generalized strains $\boldsymbol{\delta}$q, displacements rates $\boldsymbol{\delta u}$, constant (dead) loads $\mathbf{F}_c$, and variable (live) loads $\mathbf{F}_v$. Finally, the load factor α is defined, measuring the amount of the variable load vector applied. The load factor is the limit (minimum) value that the analyst wants to determine and is associated with collapse.

With the above notation, the total load vector $\mathbf{F}$ is given by

$$\mathbf{F} = \mathbf{F}_c + \alpha\mathbf{F}_v \tag{1}$$

2.2 *Yield function*

The yield function at each joint is composed by the crushing-hinging criterion and the Coulomb criterion. For the crushing-hinging criterion, it is assumed that the normal force is equilibrated by a constant stress distribution near the edge of the joint, see Figure 1a. Here, a is half of the length of a joint and w is the width of the joint normal to the plane of the block. The stress value is f_{cef}, given by Eq. (2), borrowed from concrete limit analysis (Nielsen, 1998). Here, f_c is the compressive strength of the material, and ν is an effectiveness factor, which takes into account reductions in the compressive strength due to the fact that limit analysis assumes a rigid-plastic behavior, while, in fact, softening occurs. Eq. (3) is an expression for the effectiveness factor commonly used for concrete (Nielsen, 1998), where f_c is expressed in N/mm^2.

$$f_{cef} = \nu f_c \tag{2}$$

$$\nu = 0.7 - \frac{f_c}{200} \tag{3}$$

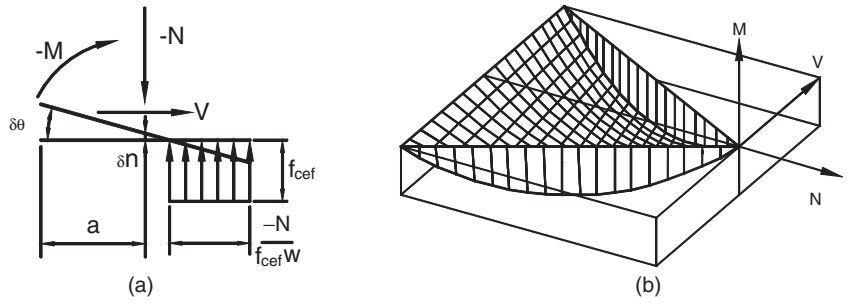

Figure 1. Joint failure: (a) generalized stresses and strains for the crushing-hinging failure mode; (b) geometric representation of a half of the yield surface.

The constant stress distribution hypothesis leads to the yield function φ given by Eq. (4), related to the equilibrium of moments; note that N_k represents a non-positive value. The Coulomb criterion is expressed by Eq. (5), related to the equilibrium of tangential forces. Here, μ is the friction coefficient or the tangent of friction angle at the joint. The equilibrium of normal forces is automatically ensured by the rectangular distribution of normal stresses. It is noted that the complete yield function is composed by four surfaces, two surfaces given by Eq. (4) and two surfaces given by Eq. (5), in view of the use of the absolute value operator. Figure 1b represents half of the yield surface ($M < 0$), while the other half ($M > 0$) is symmetric to the part shown.

$$\varphi_{1,2} \equiv N_k \left(a_k + \frac{N_k}{2 f_{cef} w_k} \right) + \left| M_k \right| \leq 0 \tag{4}$$

$$\varphi_{3,4} \equiv \mu N_k + \left| V_k \right| \leq 0 \tag{5}$$

2.3 *Flow rule*

Figure 1a illustrates also the flow mode corresponding to crushing-hinging, in agreement with the normality rule. It is noted that, for the Coulomb criterion, the flow consists of a tangential displacement only. The flow rule at a joint can be written, in matrix form, as given by Eq. (6), and, in a component-wise form, as given by Eq. (7), in which the joint subscripts have been dropped for clarity. Here, $\mathbf{N}_{0k}$ is the flow rule matrix at joint k and $\boldsymbol{\delta\lambda_k}$ is the vector of the flow multipliers, with each flow multiplier corresponding to a yield surface, and satisfying Eqs. (8-9). These equations indicate that plastic flow must involve dissipation of energy, Eq. (8), and that plastic flow cannot occur unless the stresses have reached the yield surface, Eq. (9). For the entire model, the flow rule results in Eq. (10), where the flow matrix $\mathbf{N}_0$ can be obtained by assembling all joints matrices.

$$\boldsymbol{\delta q}_k = \mathbf{N}_{0k} \boldsymbol{\delta\lambda}_k \tag{6}$$

$$\begin{bmatrix} \delta s \\ \delta n \\ \delta\theta \end{bmatrix} = \begin{bmatrix} 0 & 0 & -1 & 1 \\ a\left(1 - \dfrac{N}{f_{cef} w}\right) & a\left(1 - \dfrac{N}{f_{cef} w}\right) & 0 & 0 \\ -1 & 1 & 0 & 0 \end{bmatrix} \begin{bmatrix} \delta\lambda_1 \\ \delta\lambda_2 \\ \delta\lambda_3 \\ \delta\lambda_4 \end{bmatrix} \tag{7}$$

$$\boldsymbol{\delta\lambda}_k \geq \mathbf{0} \tag{8}$$

$$\boldsymbol{\varphi}_k^{\mathrm{T}} \boldsymbol{\delta\lambda}_k = 0 \tag{9}$$

$$\boldsymbol{\delta q} = \mathbf{N}_0 \boldsymbol{\delta\lambda} \tag{10}$$

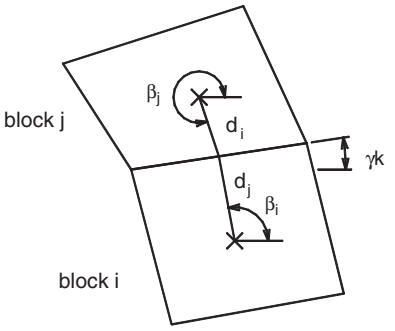

Figure 2. Representation of main geometric parameters.

2.4 *Compatibility*

Compatibility between joint k generalized strains, and the displacement rates of the adjacent blocks i and j, is given in Eq. (11), being the vector $\boldsymbol{\delta u}_i$ defined in Eq. (12) and the compatibility matrix $\mathbf{C}_{k,i}$, given in Eq. (13). Similarly, the vector $\boldsymbol{\delta u}_j$ and the matrix $\mathbf{C}_{k,j}$ can be obtained. In this last equation γ_k, β_i, β_j, are the angles between the x axis and, the direction of joint k, the line defined from the centroid of block i to the center of joint k, and the line defined from the centroid of block j to the center of joint k, respectively. Variables d_i, d_j, represent the distances from the center of joint k to the centroid of the blocks i and j, respectively, see Figure 2.

$$\boldsymbol{\delta q}_k = \mathbf{C}_{k,j}\boldsymbol{\delta u}_j - \mathbf{C}_{k,i}\boldsymbol{\delta u}_i \tag{11}$$

$$\boldsymbol{\delta u}_i^T \equiv \begin{bmatrix} \delta u_i & \delta v_i & \delta \omega_i \end{bmatrix} \tag{12}$$

$$\mathbf{C}_{k,i} = \begin{bmatrix} \cos(\gamma_k) & \sin(\gamma_k) & -d_i \sin(\beta_i - \gamma_k) \\ -\sin(\gamma_k) & \cos(\gamma_k) & d_i \cos(\beta_i - \gamma_k) \\ 0 & 0 & 1 \end{bmatrix} \tag{13}$$

Compatibility for all the joints in the model is given by Eq. (14), in which the compatibility matrix $\mathbf{C}$ is obtained by assembling the corresponding matrices for the joints of the model.

$$\boldsymbol{\delta q} = \mathbf{C}\boldsymbol{\delta u} \tag{14}$$

2.5 *Equilibrium*

Applying the contragredience principle, the equilibrium requirement is expressed by Eq. (15).

$$\mathbf{F}_c + \alpha \mathbf{F}_v = \mathbf{C}^{\mathrm{T}}\mathbf{Q} \tag{15}$$

2.6 *The mathematical programming problem*

The solution to a limit analysis problem must fulfill the previously discussed principles. In the presence of non-associated flow, there is no unique solution satisfying these principles and the actual failure load corresponds to the mechanism with a minimum load factor (Baggio and Trovalusci, 1998). The proposed mathematical description results in the non-linear programming (NLP) problem expressed in Eqs. (16–22). Here, Eq. (16) is the objective function and Eq. (17) guarantees both compatibility and flow rule. Eq. (18) is a scaling condition of the displacement rates that ensures the existence of non-zero values. This expression can be freely replaced by similar equations, as,

at collapse, the displacement rates are undefined and it is only possible to determine their relative values. Equilibrium is given by Eq. (19), and Eq. (20) is the expression of the yield condition, which together with the flow rule, Eq. (21), must fulfill Eq. (22).

Minimize: α (16)

Subject to:

$$\mathbf{N}_0 \delta\boldsymbol{\lambda} - \mathbf{C}\delta\mathbf{u} = \mathbf{0} \tag{17}$$

$$\mathbf{F}_v^{\mathrm{T}} \delta\mathbf{u} - 1 = 0 \tag{18}$$

$$\mathbf{F}_c + \alpha \mathbf{F}_v = \mathbf{C}^{\mathrm{T}}\mathbf{Q} \tag{19}$$

$$\varphi \le \mathbf{0} \tag{20}$$

$$\delta\boldsymbol{\lambda} \ge \mathbf{0} \tag{21}$$

$$\varphi^{\mathrm{T}} \delta\boldsymbol{\lambda} = 0 \tag{22}$$

This set of equations represents a case known in the mathematical programming literature as a Mathematical Problem with Equilibrium Constraints (MPEQ) (Ferris and Tin-Loi, 2001). This type of problems is hard to solve because of the complementarity constraint, Eq. (22). The solution strategy adopted here is that proposed by Ferris and Tin-Loi (2001). It consists of two phases, in the first, a Mixed Complementarity Problem (MCP), constituted by Eqs. (17–22) is solved. This gives a feasible initial solution. In the second phase, the objective function, Eq. (16), is reintroduced and Eq. (22) is substituted by Eq. (23). This equation provides a relaxation in the complementarity constraint, turns the NLP easier to solve, and allows to search for smaller values of the load factor. The relaxed NLP problem is solved for successively smaller values of ρ to force the complementarity term to approach zero.

$$-\varphi^{\mathrm{T}} \delta\boldsymbol{\lambda} \le \rho \tag{23}$$

It must be said that trying to solve a MPEQ as a NLP problem does not guarantee that the solution is a local minimum (Ferris and Tin-Loi, 2001). Nevertheless, this procedure seems computationally efficient and provides solutions of better quality than other strategies tried previously, see Orduña and Lourenço (2001).

2.7 *Computer implementation*

The main objective of this work is to develop an analysis tool suitable to be used in practical engineering projects. For this reason, the computer implementation is done resorting to AutoCAD, in which the geometry of the blocky medium is drawn. The application, developed with Visual Basic for Applications within AutoCAD (ActiveX and VBA 1999), extracts the geometric data and pre-processes it. Complementary data is added such as volumetric weight, block thickness (typically 1 m for 2D geotechnical problems), friction coefficient and compressive strength. The limit analysis is done within the modeling environment GAMS (GAMS, 1998), which allows the user to develop large and complex mathematical programming models, and solve them with state of the art routines. The previously mentioned CAD package is used as post-processor to draw failure mechanisms.

2.8 *Application*

Validation of the formulation and the implementation of the 2D model is given in Orduña and Lourenço (2003), while the extension to 3D is fully detailed in Orduña and Lourenço (2005a,b). Here, to demonstrate the applicability of limit analysis to geotechnical problems, an example of

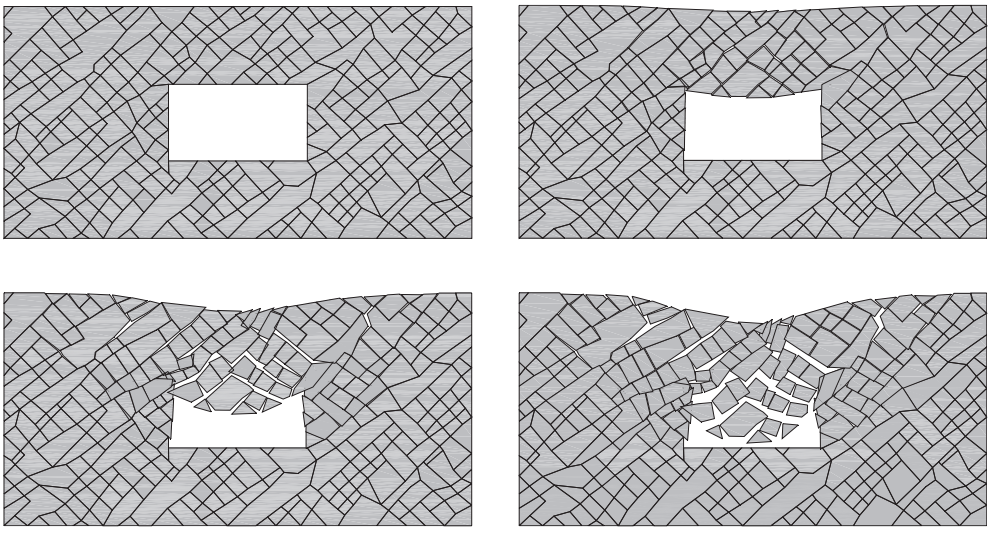

Figure 3. Evolution of a possible collapse mechanism in a tunnel excavated in a jointed rock mass.

shallow depth tunnel in fractured rock under increasing surface loads is simulated in Figure 3, see Jing (1998) for additional details. The problem geometry is formed by a rectangular domain containing two sets of random fractures. A rectangular tunnel is assumed to be excavated at the centre of the area. A vertical downward load due to self-weight appears and the other three boundaries are fixed in their respective normal directions. This problem has no practical implications and just serves as a demonstration.

3 HOMOGENIZATION TECHNIQUES

The chief disadvantage of the methods addressed in the previous section is the requirement for knowing the exact geometry of fracture systems in the problem domain. This condition can rarely be met in practice. This difficulty, however, exists for all mathematical models including those based on a continuum approach. The difference is how different approaches deal with this intrinsic difficulty. The continuum approach chooses to trade the geometrical simplicity over the material complexity by introducing complex constitutive laws and properties for an equivalent continuum through a proper homogenization process, which is only valid on the foundation of a "representative elementary volume"(REV). If this REV cannot be found or becomes too large (larger than the size of the excavation concerned, for example) then the continuum approach cannot be justified. But, in several cases, the continuum approach can be of relevance. Here, the problem of layered natural or reinforced soils is addressed by means of homogenization techniques.

3.1 *General considerations*

Composite materials consist of two or more different materials that form regions large enough to be regarded as continua and which are usually bonded together by an interface. Two kinds of information are needed to determine the properties of a composite material: the internal constituents' geometry and the physical properties of the phases. Many natural and artificial materials are immediately recognized to be of this nature, such as: laminated composites (as used in the aerospace and tire industry), alloys, porous media, cracked media (as jointed rocked masses), masonry, laminated wood, etc. However a lot of composite materials are normally assumed homogeneous. For example, this is the case of concrete, even if at a meso-level aggregates and matrix are already recognizable, and metals, in fact polycrystalline aggregates.

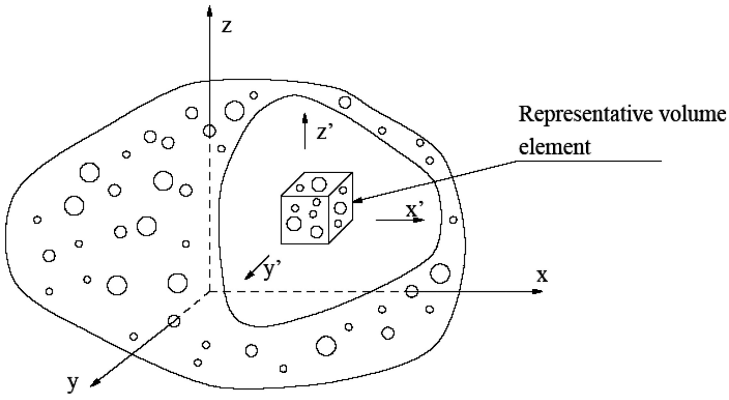

Figure 4. Representative volume element in a composite body.

The existence of randomly distributed constituents was one of the first problems to be discussed by researchers, see Paul (1960), Hashin and Shtrikman (1962) and Hill (1963). The Hashin-Shtrikman bounds were derived from a variational principle and knew some popularity but they are only valid for arbitrary statistically isotropic phase geometry, see Figure 4. An additional condition for the practical use of these bounds is that the constituents stiffness ratios are small, see Hashin and Shtrikman (1962) and Watt and O'Connell (1980). They cannot obviously provide good estimates for extreme constituent stiffness ratios such as one rigid phase or an empty phase (porous or cracked media). This precludes the use of the above results for inelastic behavior where extremely large stiffness ratios will be found.

The basis underlying the above approach is however important. It is only natural that techniques to regard any composite as an homogeneous material are investigated, provided that the model size is substantially larger than the size of the inhomogenities. In fact all phenomena in a composite material are described by differential equations with rapidly oscillating coefficients. This renders numerical solutions practically impossible since too small meshes must be considered.

Consequently, effective constitutive relations of composite structures are of great importance in the global analysis of this type of media by numerical techniques (e.g. the Finite Elements Method). For this reason the rather complicated structure of a particular composite type is replaced by an effective medium by using a technique known as homogenization method or effective medium theory. Several mathematical techniques of different complexity are available to solve the problem, Sanchez-Palencia (1980, 1987), Suquet (1982) but for periodic structures the method of "Asymptotic Analysis" has renown some popularity, see also Bakhvalov and Panasenko (1989) and Bensoussan *et al.* (1978). The extension of these methods to inelastic behavior is however not simple. Knowledge of the actual macro- or homogenized constitutive law requires knowledge of an infinite number of internal variables, namely the whole set of inelastic micro-strains. However some simplified models with piecewise constants inelastic strains can be proposed (as carried out in this paper).

The objective of the homogenization process is to describe the composite material behavior from the behavior of the different components. This problem has known a large importance in the last decade due to the increasing use and manufacture of composites. To solve the present problem some simplifications are necessary and attention is given only to the special case of laminated or layered composites. This means that the geometry of the phases are known, which simplifies enormously the task of finding equivalent elastic properties for the medium. The composite material examined is made of laminae stacked at various orientations, the only restriction being imposed on the periodicity of the lamination along the structures (see Figure 5), which is usually fulfilled in numerous engineering applications. Examples include aerospace industries, laminated wood, stratified or sedimentary soils, stratified rock masses, etc.

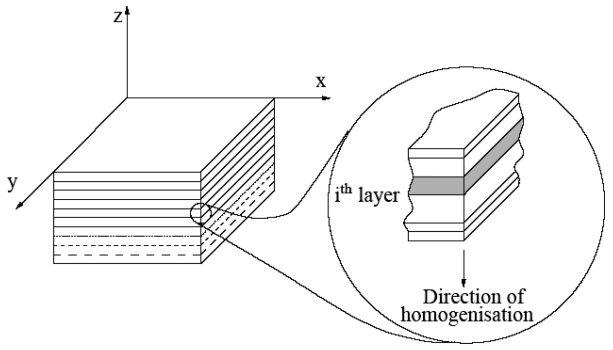

Figure 5. The periodic laminated composite material and the structure of the unit cell.

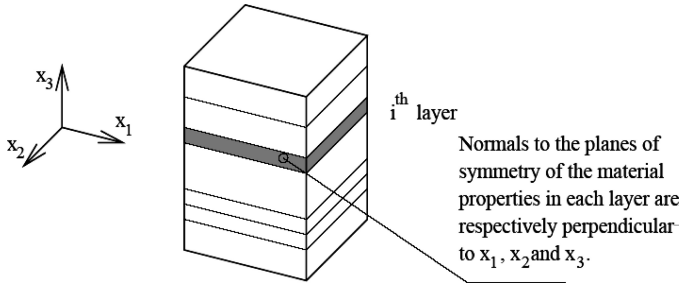

Figure 6. Unit cell. Representative prism for system of parallel orthotropic layers.

3.2 *Theory*

In the previous section a reference is made to the mathematical techniques of homogenization of periodic structures. The asymptotic expansion of the displacement and stress fields is used for example in Paipetis *et al.* (1993) to obtain the elastic stiffness of a homogenized continuum. The solution is however presented in an explicit form for each coefficient of the stiffness matrix. This solution is not practical for computational implementation and almost precludes the use of homogenization techniques for inelastic behavior.

Here, the approach originated in the field of rock mechanics will be discussed, see Salamon (1968) and Gerrard (1982), and recast in matrix form. For that purpose the layered material shown in Figure 5 is considered again, built from a repeating system of parallel layers, each of which consists of orthotropic elastic material. This means that the material properties of each layer have three mutually perpendicular planes of symmetry. The layers are aligned so that each set of three planes are respectively perpendicular to a single set of Cartesian coordinates (x_1, x_2 and x_3). The notation selected for the axes is intentionally different than the usual (x, y, z axes) to draw the attention to the fact that the x_1, x_2 and x_3 axes are placed on the material symmetry axes. The unit cell, in the form of a representative prism, is shown in Figure 6. The homogenization direction (x_3) is normal to the layering planes and, hence, for each layer, one of the planes of elastic symmetry is parallel to the layering planes. In this direction the dimension of the prism is defined by the periodicity of the structure and in the other two directions a unit length can be assumed.

It is assumed that the system of layers remains continuous after deformation and that no relative displacement takes place in the interfaces between layers. The latter assumption simplifies the problem to great extent but, at least mathematically, discontinuities in the displacements field can be incorporated, see Bakhalov and Panasenko (1989). The prism representative of the composite material is further assumed to be subjected to homogeneous distributions of stress and strain, meaning that the volume of the prism must be sufficiently small to make negligible, in the equivalent

medium, the variation of stresses and strains across it. The objective is to obtain a macro- or homogenized constitutive relation between homogenized stresses $\boldsymbol{\sigma}$ and homogenized strains $\boldsymbol{\varepsilon}$,

$$\boldsymbol{\sigma} = \boldsymbol{D}^h \boldsymbol{\varepsilon}\,, \tag{24}$$

where $\boldsymbol{D}^h$ is the homogenized stiffness matrix.

3.3 *Elastic formulation*

The macro-constitutive relation is obtained from the micro-constitutive relations. For the *ith* layer the relation between the (micro-)stress $\boldsymbol{\sigma}_i$ and the (micro-)strains $\boldsymbol{\varepsilon}_i$ is given by the (micro)stiffness matrix $\boldsymbol{D}_i$ and reads

$$\boldsymbol{\sigma}_i = \boldsymbol{D}_i \boldsymbol{\varepsilon}_i\,. \tag{25}$$

In order to establish the relationships between stresses and strains in a homogenized continuum, the following averaged quantities in an equivalent prism are defined:

$$\sigma_j = \frac{1}{V}\int_V (\sigma_j)_i\, dV = \frac{1}{V}\sum_i \int_{V_i} (\sigma_j)_i\, dV \quad ; \quad \varepsilon_j = \frac{1}{V}\int_V (\varepsilon_j)_i\, dV = \frac{1}{V}\sum_i \int_{V_i} (\varepsilon_j)_i\, dV \tag{26}$$

where V is the volume of the representative prism and j indicates all the components of the stress and strain tensors.

Auxiliary stresses (t_1, t_2 and t_{12}) and auxiliary strains (e_3, e_{13} and e_{23}) are introduced as a deviation measure of the *ith* layer stress/strain state from the averaged values. Under the assumptions given above, the stress components for the *ith* layer read

$$\begin{aligned} &\sigma_{1i} = \sigma_1 + t_{1i} \quad ; \quad \sigma_{2i} = \sigma_2 + t_{2i} \quad ; \quad \sigma_{3i} = \sigma_3 \\ &\tau_{12i} = \tau_{12} + t_{12i} \quad ; \quad \tau_{13i} = \tau_{13} \quad ; \quad \tau_{23i} = \tau_{23} \end{aligned} \tag{27}$$

and the strain components for the *ith* layer read

$$\begin{aligned} &\varepsilon_{1i} = \varepsilon_1 \quad ; \quad \varepsilon_{2i} = \varepsilon_2 \quad ; \quad \varepsilon_{3i} = \varepsilon_3 + e_{3i} \\ &\gamma_{12i} = \gamma_{12} \quad ; \quad \gamma_{13i} = \gamma_{13} + e_{13i} \quad ; \quad \gamma_{23i} = \gamma_{23} + e_{23i} \end{aligned}\,. \tag{28}$$

Now let the thickness of the *ith* layer be h_i and the normalized thickness p_i be defined as

$$p_i = \frac{h_i}{L} \tag{29}$$

where L is the length of the representative prism in the x_3 direction. Substitution of Eqs. (27) in Eqs. (26.1) yields the following conditions for the auxiliary stress components:

$$\sum p_i t_{1i} = 0 \quad ; \quad \sum p_i t_{2i} = 0 \quad ; \quad \sum p_i t_{12i} = 0 \tag{30}$$

Similarly, from Eqs. (28) and Eqs. (26.2), the auxiliary strain components are constraint by

$$\sum p_i e_{3i} = 0 \quad ; \quad \sum p_i e_{13i} = 0 \quad ; \quad \sum p_i e_{23i} = 0 \tag{31}$$

Note that, if the conditions given in the above equations are fulfilled, then the strain energy stored in the representative prism and the equivalent prism are the same.

A vector of auxiliary stresses is now defined as $\boldsymbol{t}_i$, given by

$$\boldsymbol{t}_i = (t_{1i}, t_{2i}, t_{3i}, t_{12i}, t_{23i}, t_{13i})^T\,, \tag{32}$$

and the vector of auxiliary strains $\mathbf{e}_i$ is defined as

$$\boldsymbol{e}_i = (e_{1i}, e_{2i}, e_{3i}, e_{12i}, e_{23i}, e_{13i})^T . \tag{33}$$

It is noted that half of the components of the auxiliary stress and strain vectors are zero, see Eqs. (27,28). If the non-zero components are assembled in a vector of unknowns, $\mathbf{x}_i$, defined as

$$\boldsymbol{x}_i = \boldsymbol{P}_t \boldsymbol{t}_i + \boldsymbol{P}_e \boldsymbol{e}_i , \tag{34}$$

where the projection matrix into the stress space, $\boldsymbol{P}_t$, and the projection matrix into the strain space, $\boldsymbol{P}_e$, read

$$\boldsymbol{P}_t = diag\{0,1,1,0,1,0\} \quad \text{and} \quad \boldsymbol{P}_e = diag\{1,0,0,1,0,1\} \tag{35}$$

for homogenization along the axis x_1,

$$\boldsymbol{P}_t = diag\{1,0,1,0,0,1\} \quad \text{and} \quad \boldsymbol{P}_e = diag\{0,1,0,1,1,0\} \tag{36}$$

for homogenization along the axis x_2 and

$$\boldsymbol{P}_t = diag\{1,1,0,1,0,0\} \quad \text{and} \quad \boldsymbol{P}_e = diag\{0,0,1,0,1,1\} \tag{37}$$

for homogenization along the axis x_3.

Now, the auxiliary stresses can be redefined as

$$\boldsymbol{t}_i = \boldsymbol{P}_t \boldsymbol{x}_i \tag{38}$$

and the auxiliary strains as

$$\boldsymbol{e}_i = \boldsymbol{P}_e \boldsymbol{x}_i \tag{39}$$

The stresses and strains in the *ith* layer read

$$\boldsymbol{\sigma}_i = \boldsymbol{\sigma} + \boldsymbol{t}_i \quad \text{and} \quad \boldsymbol{\varepsilon}_i = \boldsymbol{\varepsilon} + \boldsymbol{e}_i . \tag{40}$$

Incorporating these equations in Eq. (25) leads to

$$\boldsymbol{\sigma} + \boldsymbol{t}_i = \boldsymbol{D}_i (\boldsymbol{\varepsilon} + \boldsymbol{e}_i) . \tag{41}$$

By using Eqs. (38, 39), further manipulation yields

$$\boldsymbol{x}_i = (\boldsymbol{P}_t - \boldsymbol{D}_i \boldsymbol{P}_e)^{-1} (\boldsymbol{D}_i \boldsymbol{\varepsilon} - \boldsymbol{\sigma}) , \tag{42}$$

which can be recast as

$$\mathbf{0} = \sum_i p_i \boldsymbol{x}_i = \sum_i p_i (\boldsymbol{P}_t - \boldsymbol{D}_i \boldsymbol{P}_e)^{-1} (\boldsymbol{D}_i \boldsymbol{\varepsilon} - \boldsymbol{\sigma}) , \tag{43}$$

This equation yields, finally, the relation between averaged stresses and strains, as

$$\boldsymbol{\sigma} = \boldsymbol{D}^h \boldsymbol{\varepsilon} , \tag{44}$$

Here, the homogenized linear elastic stiffness matrix, $\boldsymbol{D}^h$, reads

$$\boldsymbol{D}^h = \left[\sum_i p_i (\boldsymbol{P}_t - \boldsymbol{D}_i \boldsymbol{P}_e)^{-1} \right]^{-1} \sum_i p_i (\boldsymbol{P}_t - \boldsymbol{D}_i \boldsymbol{P}_e)^{-1} \boldsymbol{D}_i \,. \tag{45}$$

Once the averaged stresses and strains are known, also the stresses and strains in the *ith* layer can be calculated. Using Eq. (42), the vector of unknowns $\boldsymbol{x}_i$ can be calculated. Algebraic manipulation yields

$$\boldsymbol{\sigma}_i = \boldsymbol{T}_{ti} \boldsymbol{\sigma} \tag{46}$$

and

$$\boldsymbol{\varepsilon}_i = \boldsymbol{T}_{ei} \boldsymbol{\varepsilon} \tag{47}$$

Here, the transformation matrices $\boldsymbol{T}_{ti}$ and $\boldsymbol{T}_{ei}$ read

$$\begin{aligned} \boldsymbol{T}_{ti} &= \boldsymbol{I} + \boldsymbol{P}_t (\boldsymbol{P}_t - \boldsymbol{D}_i \boldsymbol{P}_e)^{-1} (\boldsymbol{D}_i \boldsymbol{D}^{h^{-1}} - \boldsymbol{I}) \\ \boldsymbol{T}_{ei} &= \boldsymbol{I} + \boldsymbol{P}_e (\boldsymbol{P}_t - \boldsymbol{D}_i \boldsymbol{P}_e)^{-1} (\boldsymbol{D}_i - \boldsymbol{D}^h) \end{aligned} \tag{48}$$

where **I** is the identity matrix.

3.4 *Elastoplastic formulation*

For plasticity the form of the elastic domain is defined by a yield function $f < 0$. Loading/ unloading can be conveniently established in standard Kuhn-Tucker form by means of the conditions

$$\lambda \geq 0 \,,\; f \leq 0 \;\text{ and }\; \lambda f = 0 \tag{49}$$

where $\dot{\lambda}$ is the plastic multiplier rate. Here it will be assumed that the yield function is of the form

$$f(\boldsymbol{\sigma}, \kappa) = \Phi(\boldsymbol{\sigma}) + \overline{\sigma}(\kappa) \tag{50}$$

where κ is introduced as a measure for the amount of hardening or softening and Φ, $\overline{\sigma}$ represent generic functions. The usual elastoplastic relation hold: the total strain increment $\Delta\varepsilon$ is decomposed into an elastic, reversible part $\Delta\varepsilon^e$ and a plastic, irreversible part $\Delta\varepsilon^p$

$$\Delta\boldsymbol{\varepsilon} = \Delta\boldsymbol{\varepsilon}^e + \Delta\boldsymbol{\varepsilon}^p \tag{51}$$

the elastic strain increment is related to the stress increment by the elastic constitutive matrix D as

$$\Delta\boldsymbol{\sigma} = \boldsymbol{D} \Delta\boldsymbol{\varepsilon}^e \tag{52}$$

and the assumption of associated plasticity yields

$$\Delta\boldsymbol{\varepsilon}^p = \Delta\lambda \frac{\partial f}{\partial \boldsymbol{\sigma}} \,. \tag{53}$$

The scalar κ introduced before reads, in case of strain hardening,

$$\Delta\kappa = \sqrt{{}^2/_3 (\Delta\boldsymbol{\varepsilon}^p)^T \boldsymbol{Q}\, \Delta\boldsymbol{\varepsilon}^p} \;\;, \tag{54}$$

where the diagonal matrix $\boldsymbol{Q} = diag\{\, 1, 1, 1, ½, ½, ½, ½\}$, and, in case of work hardening,

$$\Delta\kappa = \frac{1}{\sigma} \boldsymbol{\sigma}^T \Delta\boldsymbol{\varepsilon}^p \;\;, \tag{55}$$

The integration of the constitutive equations above is a problem of evolution that can be regarded as follows. At a stage n the total strain and plastic strain fields as well as the hardening parameter(s) (or equivalent plastic strain) are known:

$$\{\boldsymbol{\varepsilon}_n, \boldsymbol{\varepsilon}_n^p, \boldsymbol{\kappa}_n\} \quad \text{given data.} \tag{56}$$

Note that the elastic strain and stress fields are regarded as dependent variables that can be always be obtained from the basic variables through the relations

$$\boldsymbol{\varepsilon}_n^e = \boldsymbol{\varepsilon}_n - \boldsymbol{\varepsilon}_n^p \quad \text{and} \quad \boldsymbol{\sigma}_n = \boldsymbol{D}\,\boldsymbol{\varepsilon}_n^e. \tag{57}$$

Therefore, the stress field at a stage $n+1$ is computed once the strain field is known. The problem is strain driven in the sense that the total strain $\boldsymbol{\varepsilon}$ is trivially updated according to the exact formula

$$\boldsymbol{\varepsilon}_{n+1} = \boldsymbol{\varepsilon}_n + \Delta\boldsymbol{\varepsilon}_{n+1}. \tag{58}$$

It remains to update the plastic strains and the hardening parameter(s). These quantities are determined by integration of the flow rule and hardening law over the step $n \rightarrow n+1$. In the frame of a fully implicit Euler backward integration algorithm this problem is transformed into a constrained optimization problem governed by discrete Kuhn-Tucker conditions as shown by Simo *et al* (1988).

It has been shown in different studies, e.g. Ortiz and Popov (1985) and Simo and Taylor (1986), that the implicit Euler backward algorithm is unconditionally stable and accurate for J2-plasticity.

This algorithm results in the following discrete set of equations:

$$\begin{aligned}
&\boldsymbol{\varepsilon}_{n+1} = \boldsymbol{\varepsilon}_n + \Delta\boldsymbol{\varepsilon}_{n+1} \\
&\boldsymbol{\sigma}_{n+1} = \boldsymbol{\sigma}^{trial} - \Delta\lambda_{n+1}\boldsymbol{D}\left.\frac{\partial f}{\partial \boldsymbol{\sigma}}\right|_{n+1} \\
&\boldsymbol{\varepsilon}_{n+1}^p = \boldsymbol{\varepsilon}_n^p + \Delta\lambda_{n+1}\boldsymbol{D}\left.\frac{\partial f}{\partial \boldsymbol{\sigma}}\right|_{n+1} \\
&\boldsymbol{\kappa}_{n+1} = \boldsymbol{\kappa}_n + \Delta\boldsymbol{\kappa}_{n+1}
\end{aligned}, \tag{59}$$

in which $\Delta\kappa_{n+1}$ results from Eq. (54) or Eq. (55) and the elastic predictor step returns the value of the elastic trial stress σ trial

$$\boldsymbol{\sigma}^{trial} = \boldsymbol{\sigma}_n + \boldsymbol{D}\,\Delta\boldsymbol{\varepsilon}_{n+1}\,, \tag{60}$$

Application of the above algorithm to the homogenized material equivalent to the layered material shown in Figure 6 results in increasing difficulties. The homogenized material consists of several layers with individual elastic and inelastic properties. As given in Eqs. (46–47), different stresses and strains are obtained for each layer, which are again different from the average stresses and strains.

Due to this feature and the fact that inelastic behavior is considered for the layers, for a given strain increment in the equivalent material it is not possible to calculate immediately the correspondent strain increments for each layer. This precludes the use of a standard plasticity algorithm due to the fact that the algorithm is strain driven. An equivalent return mapping must be carried out, in which all the layers are considered simultaneously. The equivalent return mapping is, therefore, a return mapping in all the layers (or a return mapping in terms of average strains and average stresses). This has some similitude with the fraction model, Besseling (1958).

Here only the simple case of J2-plasticity is addressed, being the reader addressed to Lourenço (1995) for other cases. The Von Mises yield criterion can be written in a matrix form and reads

$$f = ({}^3/_2\,\boldsymbol{\sigma}^T\boldsymbol{P}\,\boldsymbol{\sigma})^{1/2} - \overline{\sigma}(\kappa)\,, \tag{61}$$

where the projection matrix $\boldsymbol{P}$ reads

$$\boldsymbol{P} = \begin{bmatrix} {}^{2}/_{3} & -{}^{1}/_{3} & -{}^{1}/_{3} & 0 & 0 & 0 \\ -{}^{1}/_{3} & {}^{2}/_{3} & -{}^{1}/_{3} & 0 & 0 & 0 \\ -{}^{1}/_{3} & -{}^{1}/_{3} & {}^{2}/_{3} & 0 & 0 & 0 \\ 0 & 0 & 0 & 2 & 0 & 0 \\ 0 & 0 & 0 & 0 & 2 & 0 \\ 0 & 0 & 0 & 0 & 0 & 2 \end{bmatrix} . \tag{62}$$

For this yield surface, holds the well-known relation

$$\Delta\kappa = \Delta\lambda \ , \tag{63}$$

both for a strain or work hardening rule. From the standard algorithm shown above, cf. eq. (59), it is straightforward to obtain the update of the stress vector $\boldsymbol{\sigma}_{n+1}$ as

$$\boldsymbol{\sigma}_{n+1} = \boldsymbol{A}\,\boldsymbol{\sigma}^{trial} , \tag{64}$$

where the mapping matrix $\boldsymbol{A}$ reads

$$\boldsymbol{A} = \left[\boldsymbol{I} + \frac{3\Delta\lambda_{n+1}}{2\bar{\sigma}_{n+1}} \boldsymbol{D}\,\boldsymbol{P} \right]^{-1} , \tag{65}$$

Note that the mapping matrix is only a function of $\Delta\lambda_{n+1}$, i.e. $\boldsymbol{A} = \boldsymbol{A}(\Delta\lambda_{n+1})$. If the individual layers are considered, Eq. (64) for the ith layer must be rewritten as

$$\boldsymbol{\sigma}_{n+1,i} = \boldsymbol{A}_i\,\boldsymbol{\sigma}_i^{trial} , \tag{66}$$

where the mapping matrix, $\boldsymbol{A}_i$, is a function of $\Delta\lambda_{n+1,i}$ and the elastic trial stress σ_i^{trial}, cf. Eq. (60), reads

$$\boldsymbol{\sigma}_i^{trial} = \boldsymbol{\sigma}_{n,i} + \boldsymbol{D}_i\,\Delta\boldsymbol{\varepsilon}_{n+1,i} , \tag{67}$$

If all the layers are now considered simultaneously, the question arises whether one particular layer is elastic or plastic, but this will be considered trivial in the present note. In fact, in case of an elastic layer, Eq. (67) remains valid if the mapping matrix is redefined as the identity matrix (i.e. $\Delta\lambda_{n+1} = 0$),

$$\boldsymbol{A}_i = \boldsymbol{I} \quad \text{(if layer is elastic).} \tag{68}$$

Inserting Eq. (40) in Eq. (66), the latter can be rewritten in terms of average stresses and strains ($\boldsymbol{\sigma}$ and $\boldsymbol{\varepsilon}$) and auxiliary stresses and strains of the *ith* layer ($\boldsymbol{t}_i$ and $\boldsymbol{e}_i$) at stage $n+1$ as

$$\boldsymbol{\sigma}_{n+1} + \boldsymbol{t}_{n+1,i} = \boldsymbol{A}_i(\boldsymbol{\sigma}_n + \boldsymbol{D}_i\Delta\boldsymbol{\varepsilon}_{n+1} + \boldsymbol{D}_i\Delta\boldsymbol{e}_{n+1,i}) \ . \tag{69}$$

If a modified trial stress for the *ith* layer is defined as

$$\bar{\boldsymbol{\sigma}}_i^{trial} = \boldsymbol{\sigma}_{n,i} + \boldsymbol{D}_i\,\Delta\boldsymbol{\varepsilon}_{n+1} , \tag{70}$$

(note that the average strain is included in the expression instead of the strain of the ith layer), Eq. (69) reads

$$\boldsymbol{\sigma}_{n+1} + \boldsymbol{t}_{n+1,i} = \boldsymbol{A}_i(\bar{\boldsymbol{\sigma}}_i^{trial} + \boldsymbol{D}_i\Delta\boldsymbol{e}_{n+1,i}) \ . \tag{71}$$

Inserting Eqs. (38,39) in this equation and further manipulation, see Lourenço (1996), leads to the update of the average stress as

$$\boldsymbol{\sigma}_{n+1} = \left[\sum_i p_i (\boldsymbol{P}_t - \boldsymbol{A}_i \boldsymbol{D}_i \boldsymbol{P}_e)^{-1} \right]^{-1} \sum_i p_i (\boldsymbol{P}_t - \boldsymbol{A}_i \boldsymbol{D}_i \boldsymbol{P}_e)^{-1} \boldsymbol{A}_i \bar{\boldsymbol{\sigma}}_i^{trial} \ . \tag{72}$$

Note that the summation above is extended to all the layers (elastic and plastic). The return mapping procedure is now established in a standard way. From the average stresses it is possible to calculate the stresses in the *ith* layer. At this point it is clear that a system of non-linear equations in $\Delta\lambda_{n+1}$'s can be built: $f_i(\Delta\lambda_{n+1,1}, \ldots, \Delta\lambda_{n+1,j}) = 0$, $i = 1, \ldots, j$. This system of non-linear equations can be solved by any mathematical standard technique and has so many unknowns (and equations) as the number of plastic layers. Finally, when convergence is reached the state variables ($\boldsymbol{\varepsilon}$, $\boldsymbol{\varepsilon}_p$ and κ) can be updated. For a discussion of the algorithm implementation and the calculation of the consistent tangent operator the reader is referred to Lourenço (1996).

3.5 *Extension to a Cosserat continuum*

Physical arguments in favor of a Cosserat approach in granular materials have been put forward in Mühlhaus and Vardoulakis (1987). However, the very important feature of a Cosserat continuum is the introduction of a characteristic length in the constitutive description, thus rendering the governing set of equations elliptic while allowing for localization of deformation in a narrow, but finite band of material. The excessive dependence of standard continua upon spatial discretization can be then obviated or, at least, considerably reduced.

The implementation carried out is based on the original work of de Borst (1991, 1993) on the two-dimensional elastoplastic Cosserat continuum and the extension of Groen *et al.* (1994) to the three-dimensional case, see Lourenço (1996) for details.

3.6 *Validation*

In the following examples the described algorithm is tested by considering a material built from two layers, viz. a "weak" and a "strong" layer. Different elastic and inelastic behavior is assumed for both layers. Large scale calculations are carried out in (average) plane strain and three-dimensional applications. The objective is to assess the performance of the theory in a different class of problems ranging from highly localized to distributed failure modes. For this purpose, different calculations of the same model with increasing number of layers are carried out (note that layer in this section will be generally assumed as the repeating pattern, i.e. one layer contains two different materials, a weak and a strong layer). Convergence to the homogenized solution must be found upon increasing the number of layers.

The same fictitious material, described in Lourenço (1996), is used throughout this section. In the large calculations, 2D quadratic elements (8-noded quads) with 2×2 Gauss integration are used and 3D quadratic elements (20-noded bricks) with 3×3 Gauss integration are used. For the elastoplastic calculations a (local) full Newton-Raphson method is used in the return mapping algorithm with a 10^{-7} tolerance for all equations and a (global) full Newton-Raphson method is used to obtain convergence at global level. The tolerance is set to an energy norm of 10^{-4}.

The first example is a rigid foundation indented into a stratified soil (see Figure 7). Only half of the mesh is considered due to symmetry conditions. This example is meant to assess the performance of the homogenization technique under plane strain conditions in situations not only constrained by the material behavior, but also by geometric constraints. Clearly a localized failure is obtained around the indentation area.

A comparison is given between the 2D (plane strain) homogenized continuum and three different 2D (plane strain) layered discretizations: 8, 16 and 32 equivalent material layers (see Figure 8). Note that the zero normal strain condition introduces a three dimensional state of stress, meaning that all the calculations can be carried out under plane strain conditions. The results obtained in a

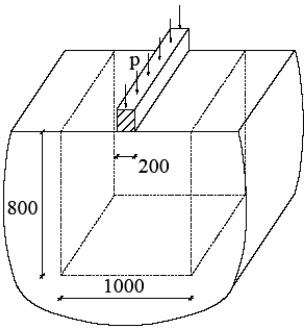

Figure 7. Geometry of rigid foundation indentation test.

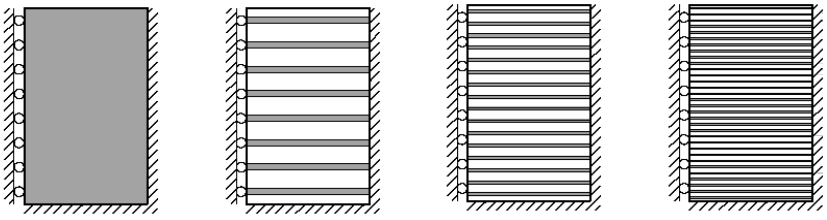

Figure 8. Different discretizations, homogenized and layered.

Table 1. Linear analysis results for $d = 1.0$ mm. Homogenized vs. layered model.

		Layered		
	Homogenized	8 layers	16 layers	32 layers
p [kN/mm]	4.056	4.170	4.074	4.020
Error	reference	2.8%	0.4%	−0.9%

linear analysis are given in Table 1 for a vertical displacement d of the foundation with a value of 1.0 mm and the different discretizations. Very good agreement is found.

The results obtained in a non-linear analysis for the different discretizations are illustrated in Figure 9. Note that all the nodes under the foundation are tied to have equal displacements. Direct displacement control of the foundation is applied in 30 equally spaced steps of 0.1 mm. The results show indeed that a convergence exists to the homogenised 2D solution with an increasing number of layers. A plateau of the force-displacement diagram was not found, even if in one the examples the calculation was carried out until a later stage ($d = 6.0$ mm). This can be due to a bad performance of the elements but, in principle, see Groen (1994), 8-noded elements with reduced integration do not show volumetric locking. The author believes that the behavior found can be explained by the geometric constraints. It is reasonable to assume that under the above circumstances the "weak layers" show (quasi) infinite hardening due to the three dimensional state of stress induced (towards the volumetric axis). From the results obtained it is clear that such behavior occurs with minor plastification of the "strong layers".

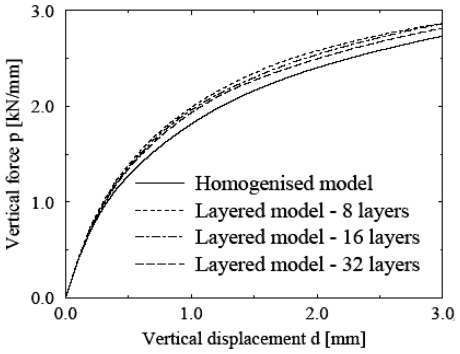

Figure 9. Force-displacement diagrams for different discretisations.

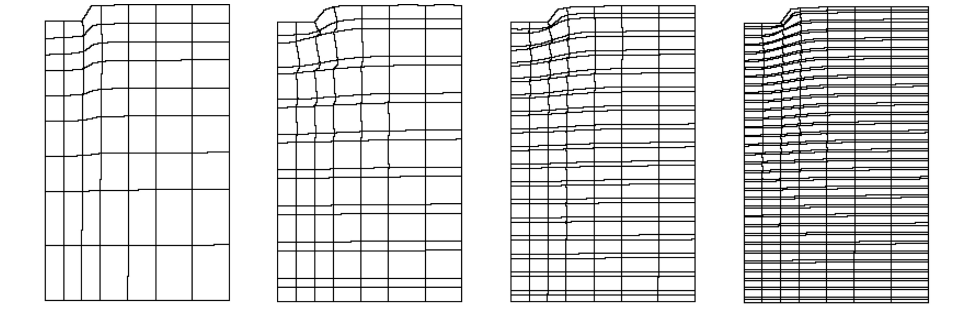

Figure 10. Deformed mesh for different discretizations ($\times 15$).

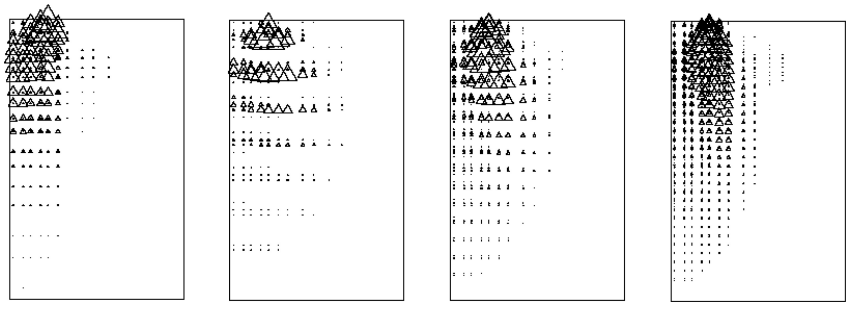

Figure 11. Equivalent plastic strain for different discretizations ($> 0.5 \times 10^{-4}$).

Fig. 10 shows the deformed meshes and Fig. 11 illustrates the plastic points at failure for the different discretizations. The deformation patterns of the layered models show some bending of the strong layers. This cannot be reproduced in the homogenized model.

It is important to point out that the foundation was assumed to be located in the middle plane of the strongest material. For examples with a small number of layers, due to the extremely large stress gradients around the geometrical discontinuities, some differences can be expected.

The collapse of a 45° slope subjected to its own weight (g) is now considered (see Figure 12). Again different discretizations are considered: the plane strain homogenized model and the plane strain layered model (4, 8 and 16 layers). The results of the maximum vertical displacement in

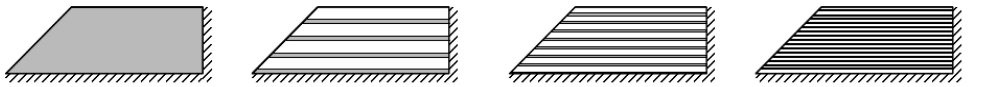

Figure 12. Different discretizations, homogenized and layered.

Table 2. Linear analysis results for $g = 1.0\,\mathrm{N/mm^3}$. Homogenized vs. layered model

		Layered		
	Homogenized	4 layers	8 layers	16 layers
Disp. y [mm]	−25.47	−27.88	−26.70	−26.09
Error	reference	9.5%	4.8%	2.4%

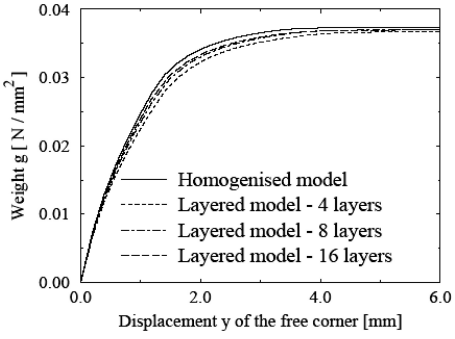

Figure 13. Force-displacement diagrams for different discretizations.

the slope obtained in a linear analysis are given in Table 2 for a weight value g with a value of $1.0\,\mathrm{N/mm^3}$ and the different discretisations. Good agreement is found.

The results obtained in a non-linear analysis for the different discretizations are illustrated in Figure 13. Indirect displacement control of the top left corner is applied in 30 equally steps of 0.2 mm. In this case even for a small number of layers the difference is minimal (1.8%). Figure 14 shows the deformed meshes and it is remarkable that such a close agreement is found in respect to the shear band formation. Figure 15 illustrates the plastic points at failure for the homogenized model in the two different materials (these results agree well with the layered model). The plastic points of the different materials are not shown in a single picture because different scales are used. The inelastic behavior of the weak material close to the bottom support is substantially larger than the diagonal shear failure.

It is important to point out that the bottom layer was assumed to be from the weak material. This has some influence on the results, especially if only a few layers are considered. This assumption is also the reason for the force-displacement diagram of the layered models being less stiff than the homogenized result (remember that the slope is subjected to self weight loading). If the bottom layer was assumed to be from the strong material, the force-displacement diagram of the layered models would be stiffer than the homogenized result.

Finally, a last example is considered in order to assess the formulation of the homogenization continuum for truly three-dimensional finite elements. For this purpose, the collapse of an embankment subjected to its own weight (g) is analyzed. Again different discretizations are considered: the 3D homogenized model and the 3D layered model with 4 and 8 equivalent material layers

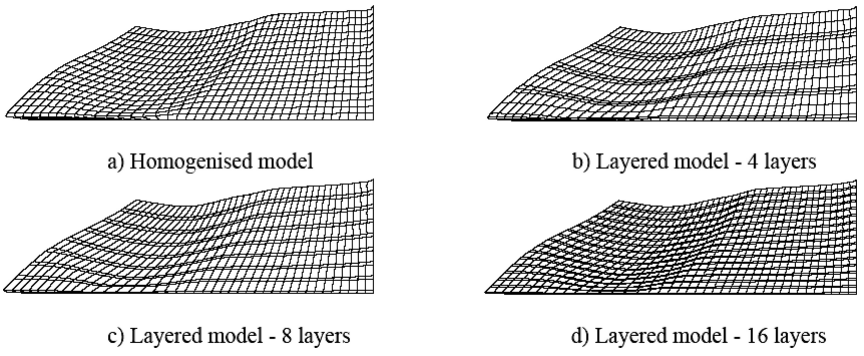

Figure 14. Deformed mesh for different discretizations (×15).

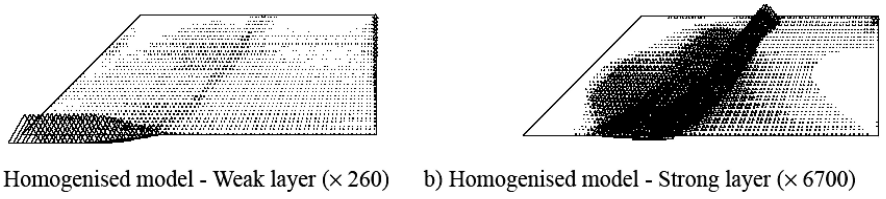

Figure 15. Equivalent plastic strain for different discretizations ($>0.5 \times 10^{-4}$).

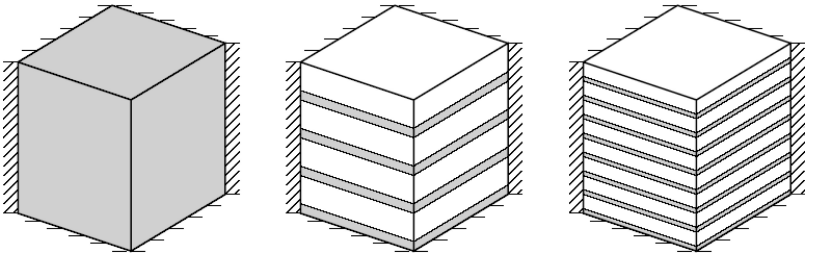

Figure 16. Different discretizations, homogenized and layered.

Table 3. Linear analysis results for $g = 1.0\,\mathrm{N/mm^3}$ (displacement of the free corner). Homogenized vs. layered model

		Layered	
	Homogenized	4 layers	8 layers
Disp. z [mm]	−29.06	−30.29	−29.63
Error	reference	4.2%	2.0%

(see Figure 16). The results obtained in a linear analysis are given in Table 3 for a weight g with a value of $1.0\,\mathrm{N/mm^3}$ and the different discretizations. Good agreement is found.

The results obtained in a non-linear analysis for the different discretizations are illustrated in Figure 17. Indirect displacement control of the free corner is applied in 20 equally spaced steps of 0.3 mm. The results show indeed that a convergence exists to the 3D homogenised solution with

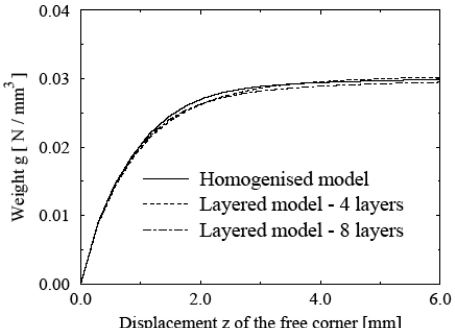

Figure 17. Force-displacement diagrams for different discretizations.

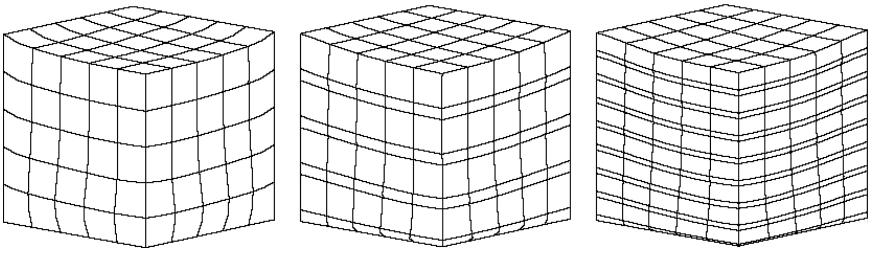

Figure 18. Total deformed mesh for different discretizations ($\times 10$).

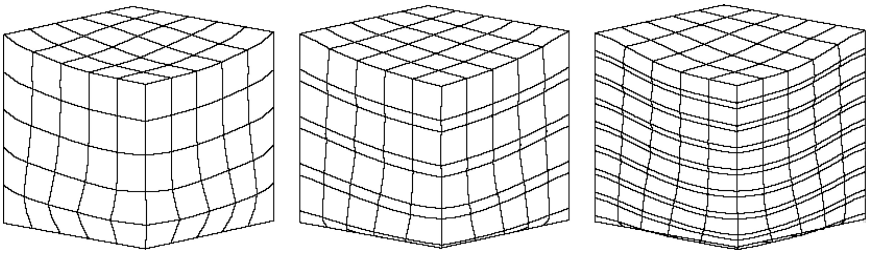

Figure 19. Incremental deformed mesh for different discretizations ($\times 300$).

an increasing number of layers. In this case even for a small number of layers the difference is minimal (1.5%). Figures 18 and 19 show the deformed meshes at failure (total and incremental) for the different discretizations. Note that, even for the incremental displacements, a good agreement is found between the 3D homogenised model and the 3D layered model (8 layers). As in the previous example, it is important to point out that the bottom layer was assumed to be from the weak material.

4 CONCLUSIONS

The difficulties involved the numerical modeling of non-homogeneous continuum media are well known. Different approaches are possible to represent heterogeneous media, namely, the discrete element method, the finite element method and limit analysis. Here, two approaches have been detailed.

The first approach considered is limit analysis of fracture or slip lines, together with individual rigid blocks. The adopted formulation assumes, besides the standard Coulomb friction law, a

compression limiter and non-associated flow. This results in a non-linear optimization problem that can be successfully solved with state of the art techniques. An example of application to the excavation of a tunnel in fractured rock is shown.

The second approach considered is the elastoplastic homogenization of layered media. A matrix formulation is proposed with straightforward extension to inelastic problems. Several examples of validation and application to stratified or reinforced soils are shown.

REFERENCES

ActiveX and VBA developer's guide. 1999. Autodesk.

Baggio, C. & Trovalusci, P. 1998. Limit analysis for no-tension and frictional three-dimensional discrete systems. *Mechanics of Structures and Machines* 26(3): 287–304.

Bakhvalov, N. & Panasenko, G. 1989. *Homogenisation: averaging processes in periodic media.* Dordrecht : Kluwer Academic Publishers.

Bensoussan, A., Lions, J.-L. & Papanicolaou, G. 1978. *Asymptotic analysis of periodic structures.* Dordrecht : Kluwer Academic Publishers.

Besseling, J.F. 1958. A theory of elastic, plastic and creep deformations of an initially isotropic material showing anisotropic strain-hardening, creep recovery and secondary creep. *J. Appl. Mech.* 22: 529–536.

Cundall, P.A. & Strack O.D.L. 1979. Discrete numerical-model for granular assemblies. *Geotechnique* 29 (1): 47–65.

de Borst, R. 1991. Simulation of strain localisation: A reappraisal of the Cosserat continuum, *Engng. Comput.* 8: 317–332.

de Borst, R. 1993. A generalisation of J2-flow theory for polar continua, *Comp. Meth. Appl. Mech. Engng.* 103: 347–362.

Ferris, M.C. & Tin-Loi, F. 2001. Limit analysis of frictional block assemblies as a mathematical program with complementarity constraints. *International Journal of Mechanical Sciences* 43: 209–224.

Fredlund D.G. & Krahn J. 1977. Comparison of slope stability methods of analysis. *Canadian Geotechnical Journal* 14 (3): 429–439.

GAMS A user's guide. 1998. Brooke, A., Kendrick, D., Meeraus, A., Raman, R. & Rosenthal, R.E. http://www.gams.com/docs/gams/GAMSUsersGuide.pdf.

Gerrard, C.M. 1982. Equivalent elastic moduli of a rock mass consisting of orthorhombic layers. *Int. J. Rock. Mech. Min. Sci. & Geomech.* 19: 9–14.

Goodman, R.E., Taylor, R.L. & Brekke T.L. 1968. A model for mechanics of jointed rock. *Journal of the Soil Mechanics and Foundations Division* 94 (3): 637–659.

Groen, A.E. 1994. *Improvement of low order elements using assumed strain concepts*. Delft : Delft University of Technology.

Groen, A.E., Schellekens, J.C.S. & de Borst, R. 1994. Three-dimensional finite element studies of failure in soil bodies using a Cosserat continuum. In: H.J. Siriwardane & M.M. Zaman (eds), *Computer Methods and Advances in Geomechanics*: 581–586. Rotterdam: Balkema.

Hart, R.D. 1991. General report: an introduction to distinct element modelling for rock engineering. In: W. Wittke (eds), *Proceedings of the of 7th Congress on ISRM*: 1881–1892. Rotterdam: Balkema.

Hashin, Z. & Shtrikman, S. 1962. On some variational principles in anisotropic and nonhomogeneous elasticity. *J. Mech. Phys. Solids* 10: 335–342.

Hill, R. 1963. Elastic properties of reinforced solids: Some theoretical principles. *J. Mech. Phys. Solids* 11: 357–372.

Jing, L. 1998. Formulation of discontinuous deformation analysis (DDA) – an implicit discrete element model for block systems. *Engineering Geology* 49: 371–381.

Lourenço, P.B. 1995. *The elastoplastic implementation of homogenization techniques: With an extension to masonry structures*. Delft : Delft University of Technology.

Lourenço, P.B. 1996. A matrix formulation for the elastoplastic homogenisation of layered materials, *Mechanics of Cohesive-Frictional Materials* 1: 273–294.

Mühlhaus, H.-B. & Vardoulakis, I. 1987. The thickness of shear bands in granular materials, *Geotechnique* 37: 271–283.

Nielsen, M.P. 1999. *Limit Analysis and Concrete Plasticity*. Boca Raton : CRC Press.

Orduña, A. & Lourenço, P.B. 2001. Limit analysis as a tool for the simplified assessment of ancient masonry structures. In P.B. Lourenço & P. Roca (eds) *Proc. 3rd Int. Seminar on Historical Constructions*: 511–520. Guimarães : Universidade do Minho.

Orduña, A. & Lourenço, P.B. 2003. Cap model for limit analysis and strengthening of masonry structures. *J. Struct. Engrg.* 129(10), 1367–1375.

Orduña, A. & Lourenço, P.B. 2005a. Three-dimensional limit analysis of rigid blocks assemblages. Part I: Torsion failure on frictional joints and limit analysis formulation. *Int. J. Solids and Structures* 42(18–19): 5140–5160.

Orduña, A. & Lourenço, P.B. 2005b. Three-dimensional limit analysis of rigid blocks assemblages. Part II: Load-path following solution procedure and validation. *Int. J. Solids and Structures* 42(18-19): 5161–5180.

Ortiz, M. & Popov, E.P. 1985. Accuracy and stability of integration algorithms for elastoplastic constitutive relations. *Int. J. Numer. Methods Engrg.* 21: 1561–1576.

Paipetis, S.A., Polyzos, D. & Valavanidis, M. 1993. Constitutive relations of periodic laminated composites with anisotropic dissipation. *Arch. Appl. Mech.* 64: 32–42.

Paul, B. 1960. Prediction of elastic constants of multiphase materials. *Trans. of AIME* 218: 36–41.

Salamon, M.D.G. 1968. *Elastic moduli of stratified rock mass*. *Int. J. Rock. Mech. Min. Sci.* 5: 519–527.

Sanchez-Palencia, E. 1980. *Non-homogeneous media and vibration theory*. Berlin: Springer.

Sanchez-Palencia, E. 1987. *Homogenization techniques for composite media*. Berlin: Springer.

Shi, G. & Goodman, R.E. 1985. Two dimensional discontinuous deformation analysis. *Int. J. Numerical Analyt. Meth. Geomech.* 9, 541–556.

Simo, J.C. & Taylor, R.L. 1986. A return mapping for plane stress elastoplasticity. *Int. J. Numer. Methods Engrg*. 22: 649–670.

Simo, J.C., Kennedy, J.G. & Govindjee, S. 1988. Non-smooth multisurface plasticity and viscoplasticity. Loading/unloading conditions and numerical algorithms. *Int. J. Numer. Methods Engrg.* 26: 2161–2185.

Suquet, P. 1982. *Plasticité et homogénéisation*. PhD Dissertation. Paris : Université de Paris.

Watt, J.P. & O'Connell, R.J. 1980. An experimental investigation of the Hashin-Shtrikman bounds on twophase aggregate elastic properties. *Physics of Earth and Planetary Interiors* 21: 359–370.